Journal of Pathology Informatics 15 (2024) 100373

Contents lists available at ScienceDirect

Journal of Pathology Informatics

journal homepage: www.elsevier.com/locate/jpi

Microcomputed tomography as a diagnostic tool for detection of lymph node metastasis in non-small cell lung cancer: A decision-support approach for pathological examination "A pilot study for method validation"

Ayten Kayı Cangır [a,b,*,1], Süleyman Gökalp Güneş [a,1], Kaan Orhan [c], Hilal Özakıncı [d], Yusuf Kahya [a], Duru Karasoy [e], Serpil Dizbay Sak [d]

[a] Department of Thoracic Surgery, Ankara University Faculty of Medicine, Ankara, Turkey
[b] Medical Design Application and Research Center (MEDITAM), Ankara University, Ankara, Turkey
[c] Department of Dentoaxillofacial Radiology, Ankara University Faculty of Dentistry, and MEDITAM, Ankara, Turkey
[d] Department of Pathology, Ankara University Faculty of Medicine, Ankara, Turkey
[e] Department of Statistics, Faculty of Science, Hacettepe University, Ankara, Turkey

ARTICLE INFO

Keywords:
Micro-CT
Lung cancer
Lymph node metastasis

ABSTRACT

Background: Non-small cell lung cancer (NSCLC) patients without lymph node (LN) metastases (pN0) may exhibit different survival rates, even when their T stage is similar. This divergence could be attributed to the current pathology practice, wherein LNs are examined solely in two-dimensional (2D). Unfortunately, adhering to the protocols of 2D pathological examination does not ensure the exhaustive sampling of all excised LNs, thereby leaving room for undetected metastatic foci in the unexplored depths of tissues. The employment of micro-computed tomography (micro-CT) facilitates a three-dimensional (3D) evaluation of all LNs without compromising sample integrity. In our study, we utilized quantitative micro-CT parameters to appraise the metastatic status of formalin-fixed paraffin-embedded (FFPE) LNs.

Methods: Micro-CT scans were conducted on 12 FFPEs obtained from 8 NSCLC patients with histologically confirmed mediastinal LN metastases. Simultaneously, whole-slide images from these FFPEs underwent scanning, and 47 regions of interest (ROIs) (17 metastatic foci, 11 normal lymphoid tissues, 10 adipose tissues, and 9 anthracofibrosis) were marked on scanned images. Quantitative structural variables obtained via micro-CT analysis from tumoral and non-tumoral ROIs, were analyzed.

Result: Significant distinctions were observed in linear density, connectivity, connectivity density, and closed porosity between tumoral and non-tumoral ROIs, as indicated by kappa coefficients of 1, 0.90, 1, and 1, respectively. Receiver operating characteristic analysis substantiated the differentiation between tumoral and non-tumoral ROIs based on thickness, linear density, connectivity, connectivity density, and the percentage of closed porosity.

Conclusions: Quantitative micro-CT parameters demonstrate the ability to distinguish between tumoral and non-tumoral regions of LNs in FFPEs. The discriminatory characteristics of these quantitative micro-CT parameters imply their potential usefulness in developing an artificial intelligence algorithm specifically designed for the 3D identification of LN metastases while preserving the FFPE tissue.

Introduction

Non-small cell lung cancer (NSCLC) is an aggressive malignancy, and lymph node (LN) metastasis of resected NSCLC is both an important negative prognostic factor and a determinant of appropriate adjuvant treatment.[1,2] The presence of LN metastases in NSCLC not only impacts adjuvant chemotherapy decisions but also influences the decision-making process for radiotherapy in N2 disease.[2–5] Accurate detection of LN status is critical. However, 30–40% of patients with stage I NSCLC experience post-operative local recurrence and distant metastasis despite histologically

Abbreviations: CT, Computed tomography; NSCLC, Non-small cell lung cancer; MLN, Mediastinal lymph nodes; LN, Lymph node; Micro-CT, Micro-computed tomography; 2D, Two-dimensional; 3D, Three-dimensional; HE, Hematoxylin and eosin; FFPE, Formalin-fixed and paraffin-embedded; ROI, Region of interest; OV/TV, Object volume; TV, Tissue volume; ST, Structural thickness; IS, Intersection surface; SMI, Structure model index; SLD, Structure linear density; Cn, Connectivity; CnD, Connectivity density.

* Corresponding author.
E-mail addresses: kayicangir@gmail.com cangir@medicine.ankara.edu.tr (A. Kayı Cangır).

[1] Contributed equally to this work.

http://dx.doi.org/10.1016/j.jpi.2024.100373
Received 8 December 2023; Received in revised form 6 March 2024; Accepted 18 March 2024
Available online 24 March 2024

confirmed curative resection and tumor-free LNs (pN0).[3,6,7] Thus, long-term survival in a major subgroup of N0 patients remains unsatisfactory.[6,7] This might be attributed to suboptimal LN dissection or inadequate histopathological evaluation.[3,8–10] Two potential explanations exist for this phenomenon: micrometastases in hematoxylin and eosin (H&E)-stained slides may have been overlooked during histopathological examination, or even though a metastatic focus is present in the deeper layers of the formalin-fixed and paraffin-embedded (FFPE) tissue, the tumor might be absent in the H&E slides. While serial sectioning of FFPEs followed by immunohistochemical examination could enhance the precision of detecting deep-seated LN metastases, this method is both time-consuming and expensive.[11]

Micro-computed tomography (micro-CT) uses cone-shaped beams for reconstruction and back-projection. The volumetric voxel size is almost 1 million-fold smaller than that of conventional CT, approximately 1–50 m, leading to detect microchanges in the tissue. Micro-CT has many applications given the good resolution and non-invasive nature of the technique.[12] The three-dimensional (3D) images allow both quantitative and qualitative evaluation.[13] Micro-CT is non-destructive and further scans and other investigations are possible. Micro-CT is widely employed by bone and dental researchers. Bone biologists have enthusiastically adopted laboratory micro-CT systems because they afford 3D views of the architecture and mechanical competence of the trabecular and cortical bones of both clinical biopsy samples and animal models of disease.[14] In any research field, micro-CT non-destructively and directly yields 3D images[15,16] with information on the internal structures of materials ranging from industrial equipment to human tissues. Micro-CT is a non-invasive ex-vivo imaging tool that reveals internal 3D structures of opaque samples at sub-micron resolution.[17] Although there is substantial literature on the use of micro-CT to characterize musculoskeletal tissues, especially in the field of dentistry, only a few studies have evaluated other human tissues.[12] Lung studies have commonly focused on small samples, both in vivo and ex vivo. When evaluating the lung specimens ex vivo, micro-CT devices operate at very small scales with high radiation doses, yielding digital images with micrometer resolution, enabling the diagnosis of pulmonary diseases that manifest at the microanatomical scale.[18–22] Micro-CT exhibits many clinical applications across a wide spectrum of pulmonary pathologies, including chronic restrictive and obstructive lung diseases as well as lung cancer; comparative studies of the human lung are rare.[23–25] Apart from high-resolution images of hard tissue samples, histometric features of the visual microarchitecture can be converted into numerical data; structural variables that can be statistically analyzed are generated from the visual microarchitectural features of tissues.

Following surgery, NSCLC patients with pN0 disease exhibit divergent survival durations, even when the tumor (T) stage is the same.[3] Beyond variations in the intrinsic biological characteristics of tumors, in some instances, this divergence may arise from the limitation of current histopathological methods to comprehensively assess all LN tissues. Micro-CT facilitates the generation of 3D images for entire FFPE tissues, providing numerical values for structural variables. This technique evaluates areas within FFPEs that aren't covered by 2D histopathological sections. Our main goal is to distinguish differences between non-tumoral and metastatic regions within FFPE blocks of LNs, using micro-CT images and extracting numerical parameters.

Materials and methods

The study was approved by the Institutional Review Board of the University Faculty of Medicine [IRB no. 16-287-19]. Twelve LN FFPE samples from eight patients diagnosed with NSCLC during routine pathology work-up were used. All patients underwent surgery in the Department of Thoracic Surgery, Ankara University Faculty of Medicine, and LN metastases were confirmed histologically. None of them received neoadjuvant treatment. H&E-stained 4–5-μm-thick sections from the 12 FFPEs were scanned using the Panoramic 250 Flash digital scanner (3DHISTECH, Budapest, Hungary). Forty-seven ROIs (17 metastatic foci, 11 normal lymphoid tissues, 10 adipose tissues, and 9 anthracofibrosis) were marked on the virtual slides by two pathologists. A different random color (red, yellow, green, blue, or gray) was assigned to each ROI on each slide to differentiate the ROIs (Fig. 1). The workflow is shown in Fig. 2.

Micro-CT

After obtaining the sections for routine pathology work-up, the FFPE block was removed from the cassette, along with the paraffin, using a knife. Following scanning, the FFPE tissue adhered to the block using liquid and hot paraffin, maintaining the tissue's original orientation. To ensure the compatibility of the micro-CT images and the virtual histopathological

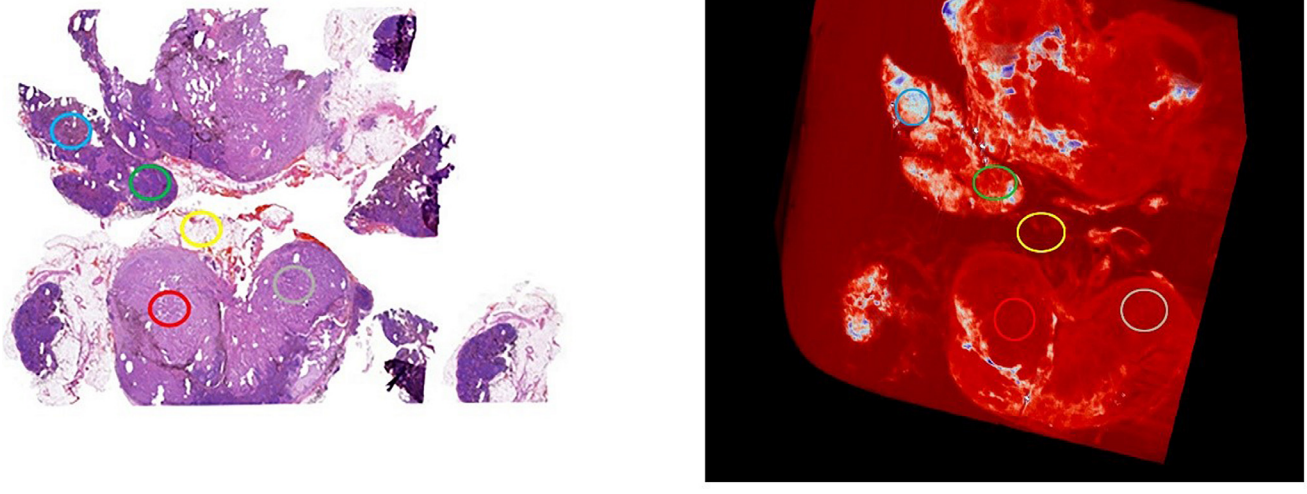

Fig. 1. Whole-slide images of three adenocarcinoma cases and the regions of interest (ROIs) that were evaluated with micro-CT for structural parameters (a–c). ROI-Cs (white circles) to represent carcinoma areas; ROI-Ns (blue circles) to represent non-tumoral pulmonary parenchyma within the same paraffin blocks. Insets show three of the ROI-Cs (HE; original magnification WSIs: 0.4×, insets:10×).

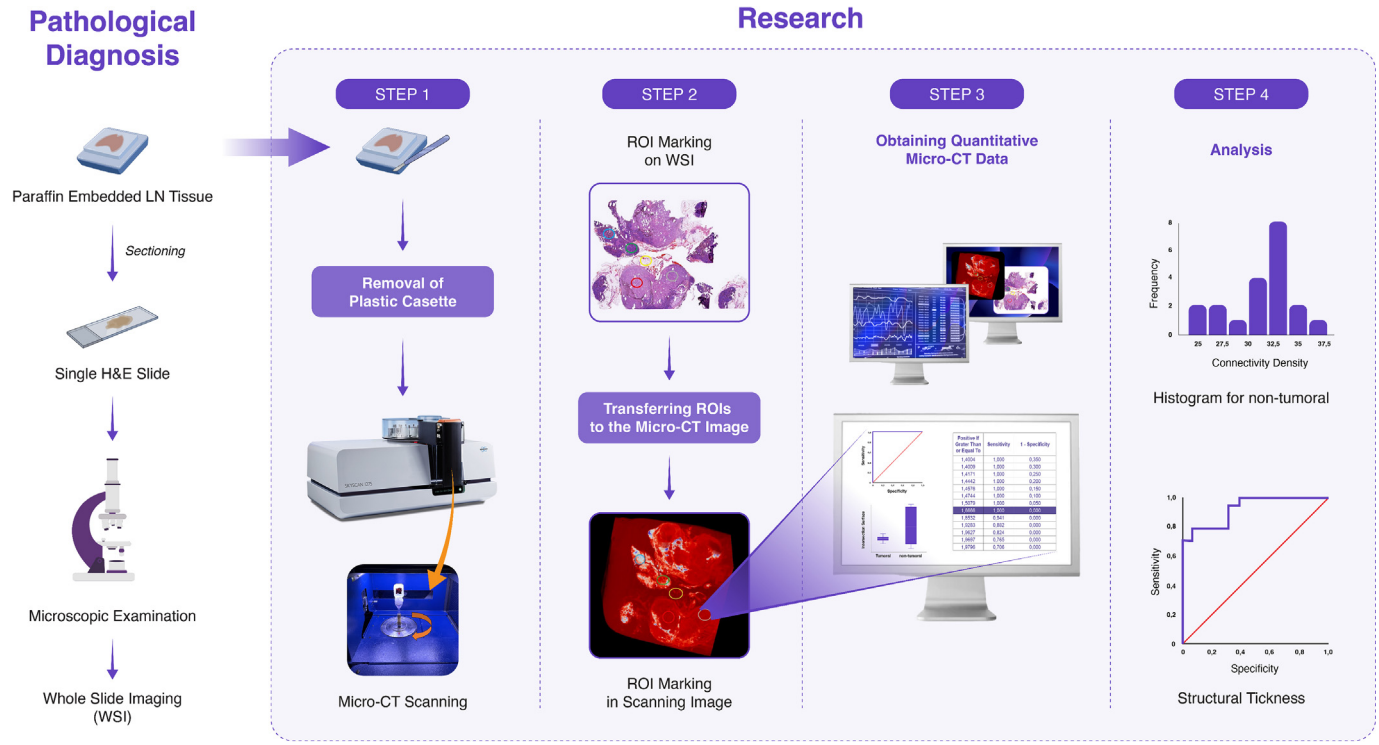

Fig. 2. Schematic view of the workflow.

slides, the FFPE tissues were placed at right angles to the blocks using a specimen holder. A high-resolution desktop micro-CT system (Bruker Skyscan 1275, Kontich, Belgium) was used to scan tissues within the blocks. The scan parameters have been described previously.[26] Before scanning and reconstruction, the beam-hardening correction and optimal contrast limits were set according to the manufacturer's instructions.

Image analysis

NRecon (ver. 1.6.10.5, SkyScan) and CTAn (ver. 1.19.11.1, SkyScan) were used for visualization and quantitative measurements. We employed a modification of the algorithm described by Feldkamp et al. to obtain axial 2D 1000 × 1000-pixel images.[27] In terms of the reconstruction variables, the ring artifact correction and smoothing were set to zero and the beam artifact correction to 40%. NRecon was used to reconstruct 2D slices of the specimens. Cross-sectional images were reconstructed from the entire volume of each paraffin block. CTAn was employed for analysis. The reconstructed images were further processed by Skyscan CTVox (ver. 3.3.1) to allow visualization by referencing the H&E-stained sections. Guided by both the virtual slides and 3D micro-CT volumes ROIs were drawn to include different areas (Fig. 1). Forty-seven ROIs were colored on both the histopathological and micro-CT images. The evaluator of the micro-CT images (KO) was blinded to the nature of the ROIs.

When differentiating metastatic areas from non-tumoral areas tissues, an appropriate threshold is required. To this end, original grayscale images were processed using a Gaussian low-pass filter for noise reduction employing a semi-automatic global threshold method. After thresholding (binarization), the images featured black and white pixels. Then, for each slice, an ROI that contained a single complete object was defined before the calculation of various parameters.

A radiologist with 15 years of experience with micro-CT (KO) performed all evaluations. The CTAn software was fully exploited when analyzing the 3D microarchitecture. We measured the percentage object volume, intersection surface, structural thickness, structural linear density, connectivity, connectivity density, and closed and open porosities; all were based on the volume of the ROI.

The percentage of object volume relative to the total tissue volume is widely used by pathologists to measure object gain or loss, i.e., the fraction of a volume of interest occupied by tissue.

Structural thickness refers to both the thickness of all tissues and the mean thickness of different tissues. The intersection surface is that of tissue contact. The software measures both the total surface area of the ROI and the extent of the ROI surface intersected by binarized tissue. This allows tissue contact surfaces to be measured at virtual ROI boundaries.

The structural linear density is any value per unit length. The term "linear density" is commonly used when describing the characteristics of 1D objects, although it is also used to describe the density of a 3D quantity in one particular dimension. Just as density is commonly taken to mean mass density, linear density often refers to linear mass density. Connectivity describes the topology of porous tissue. Connectivity density is a measure of the extent of tissue connectivity normalized to the total tissue volume. Several parameters, including the number, volume, total surface, and pore numbers and percentages, can be used to describe porosity. Pores are typically classified as closed or open. An open pore intersects with an ROI boundary and is thus connected to the outside in 2D or 3D; a closed pore does not intersect or connect. Closed pores are black pixels surrounded by a border of white pixels. We measured the percentages of closed and open pores over the entire specimen volume.

Statistical analysis

Data analyses were performed using IBM SPSS Statistics for Windows version 23. The normal distribution of data was assessed by the Shapiro–Wilk test. Two group comparisons (tumoral and non-tumoral ROIs) were performed using the independent *t*-test or the Mann–Whitney *U* test, depending on whether the data were normally distributed or not. A *p*-value less than 0.05 is considered statistically significant. K-means clustering was employed to classify patients into four different clusters and then into two clusters (tumoral and non-tumoral ROIs) based on the relevant variables. The Cohen's Kappa coefficient was used to assess the results obtained from cluster analysis. The optimal cut-off values were detected by receiver operating characteristic (ROC) analysis.

Results

Each color represented a different ROI in each FFPE to avoid bias; the data for the 47 ROIs are shown in Supplementary Table 1. Again, to avoid bias, four different clusters were blindly created based on the variables subjected to cluster analysis, and the distributions within these clusters of tumor, lymphoid, anthracofibrotic, and adipose tissue areas, were determined overall and for each variable (Table 1). Open porosity (100%) and structural linear density (94.1%) for tumor areas; connectivity (100%) and closed porosity (100%) for lymphoid tissues; intersection surface (100%), structural thickness (100%), structural linear density (100%), connectivity density (100%), and open porosity (100%) for anthracofibrotic areas; and structural thickness (100%) for adipose tissues were the parameters with the highest accuracies. When all variables were included among the four clusters, lymphoid tissue had the highest accuracy and tumor areas the lowest (Table 2). To identify the variables with high accuracy in detecting target areas, eight subgroups were formed for the seven variables in Table 2, and the analyses were repeated. In the subgroup analyses, closed and open porosities best identified tumoral and anthracofibrotic areas, while connectivity and closed porosity best identified lymphoid and adipose areas (Table 2).

As our main purpose was to identify tumor areas in LNs, using data from 37 ROIs in Supplementary Table 1, k-means clustering analyses and descriptive statistics were performed by dividing these ROIs into two groups: tumor ($n=17$) and non-tumor areas (lymphoid areas = 11 and anthracofibrotic areas = 9) (Table 3). ROC analysis revealed that tumor and non-tumor ROIs were successfully differentiated by the structural linear density, connectivity, connectivity density, and percentage of closed porosity (kappa coefficients: 1, 0.90, 1, and 1, respectively). ROC analysis also revealed that ROIs with a structural linear density >= 1.67 (sensitivity 1, specificity 1), connectivity >= 1990 (sensitivity 1, specificity 1), connectivity density >= 48.22 (sensitivity 1, specificity 1), and/or closed porosity >= 4.29% (sensitivity 1, specificity 1) were tumor areas (Supplementary Table 1).

Discussion

While NSCLC carries a fatal prognosis, early-stage patients who undergo surgery can achieve long-term survival. Those without LN metastasis (pN0) typically experience better survival rates. The 5-year survival rate for NSCLC patients with cT1/2 N0 disease ranges from 62% to 88%,[3] signifying that 12–38% of patients experience mortality within 5 years. The cause of death within this population remains ambiguous. Potential factors such as down-staging, attributed to incomplete evaluation of the entire LN FFPE, and undertreatment could be contributing to these fatalities. Adjuvant therapy is generally not recommended for patients with a tumor diameter of 4 cm and pN0 status. Conversely, pN1 or pN2 status is associated with poor survival and is an indication for adjuvant systemic therapy. In recent decades, the advent of targeted therapies and immunotherapies has significantly enhanced long-term survival rates. Consequently, factors influencing the decision to initiate adjuvant systemic treatment, particularly LN metastasis, have gained even greater significance.

Systematic LN dissection stands as a pivotal element in lung cancer surgery. The LN stations in the lung cancer staging system undergo histopathological evaluation. Typically, LNs are sliced to a thickness of approximately 2 mm, subjected to macroscopic examination for metastases, and completely embedded in paraffin blocks. Metastasis detection relies on 2D H&E-stained sections from the first layers of FFPEs. While macro-metastases are readily apparent, it is possible to miss micro-metastases lying deep in the tissue. This circumstance may, in part, elucidate the variation in survival times among N0 cases with similar T stages. In other words, some N0 cases may harbor metastatic foci within the FFPE tissue, potentially eluding detection by the pathologist. Consequently, certain pN0 cases might be pN1 or even pN2.

Although it is theoretically possible to examine the entire FFPE during routine pathology examination, this is very expensive and time-consuming. Recently, 3D reconstructions of whole-slide histological data have revealed new diagnostic patterns given the improved correlations between imaging modalities.[25] However, it remains necessary to prepare at least 100–200 serial, glass slide-mounted tissue sections.[25] Until recently, there was no non-destructive method available that allowed the preservation of tissue while evaluating an entire LN in an FFPE block. Micro-CT is a relatively new imaging method with a voxel size volumetrically almost 1 million times smaller than that of conventional computed tomography (CT) and allows researchers to collect both quantitative and qualitative information on various sample types by obtaining 3D images with sub-micron

Table 1
Detection percentage of tumor, lymphoid, anthracofibrotic and adipose tissue areas in four different clusters created by K-means clustering.

	ROI			
Variables	Tumour (n = 17) %	Lymphoid tissue (n = 11) %	Anthracofibrotic (n = 9) %	Adipose tissue (n = 10) %
1. Intersection surface	82.4	54.5	**100**	80
2. Structural thickness	64.7	81.8	**100**	**100**
3. Structural linear density	**94.1**	81.8	**100**	60
4. Connectivity	58.8	**100**	88.9	90
5. Connectivity density	52.9	63.6	**100**	90
6. Closed porosity (%)	88.2	**100**	88.9	80
7. Open porosity (%)	**100**	72.7	72.7	40

Table 2
For eight subgroups, detection percentage of tumor, lymphoid, anthracofibrotic and adipose tissue areas in four different clusters created by K-means clustering.

ROI identified in LN	Set A (%) (All)[1]	Set B (%) (1+2+3+6+7)	Set C (%) (2+3+6+7)	Set D (%) (3+6+7)	Set E (%) (6+7)	Set F (%) (3+4+6)	Set G (%) (4+5+6)	Set H (%) (4+6)
Tumour (n = 17)	58.8	**100**	**100**	**100**	**100**	58.8	58.8	58.8
Lymphoid tissue (n = 11)	**100**	72.7	72.7	72.7	72.7	**100**	**100**	**100**
Anthracofibrotic (n = 9)	88.9	**100**	**100**	**100**	**100**	88.9	88.9	88.9
Adipose tissue (n = 10)	90	50	50	50	50	90	90	**90**

[1] **Variables: 1: Intersection surface, 2: Structural thickness, 3: Structural linear density, 4: Connectivity, 5: Connectivity density, 6: Closed porosity (%), 7: Open porosity (%).**

Table 3
Kappa coefficients for the results obtained from cluster analysis, and ROC analysis results of tumoural and non-tumoural areas

Variables	Kappa coefficient	Sensitivity	Specificity	Area under the ROC curve	Cut off value
Intersection surface	0.48	0.88	0.45	0.47	31.32
Structural thickness	0.48	1.00	0.75	0.95	0.72
Structural linear density	**1**	**1.00**	**1.00**	**1.00**	**1.67**
Connectivity	**0.90**	**1.00**	**1.00**	**1.00**	**1990**
Connectivity density	**1**	**1.00**	**1.00**	**1.00**	**48.22**
Closed porosity	**1**	**1.00**	**1.00**	**1.00**	**4.29**
Open porosity	0.43	1.00	0.00	0.02	19.92

resolution through micro-CT. Micro-CT is generally used to obtain precise information about the internal structure of materials. It is known to be used in the industrial field and materials sciences such as engineering, microprocessor production, and dealing with materials such as stone and metal.[26–28] There are a few studies using micro-CT in the examination of human tissues.[15,29,30]

Micro-CT yields high-resolution 3D images along any direction within the volume of a specimen without sectioning of soft or calcified tissues and thus facilitates a better understanding of disease.[31–34] However, studies on various tissues have reported very different correlations between micro-CT and histopathological data.[35,36] Given that histomorphometric measurements are inherently 2D and micro-CT assessments provide 3D perspectives, disparities between the two methodologies are anticipated.

Micro-CT not only produces high-resolution tissue images but also allows the conversion of histometric properties from the visual microarchitecture into numerical data that can be subjected to statistical analysis. The micro-CT morphological measurements are highly correlated with histomorphometric data that serve as the gold-standard when evaluating bone microarchitecture.[37] Our study highlights the capacity of micro-CT imaging to complement—and in terms of specific diagnostic questions (tumor volume and margin), potentially even replace—slide microscopic imaging to guide clinical decisions. Although the approach differs greatly from conventional histopathological evaluation, more innovations and developments are to be expected. Radiomics and artificial intelligence applications are increasingly being used to support medical decisions. The numerical data obtained via micro-CT examination may take visual histopathological evaluation to a level at which artificial intelligence algorithms can be employed. The success of machine learning (ML) algorithms in terms of automating tasks that are not analytically well-defined indicates that such methods engage in automated feature extraction and are thus better than computer vision-based approaches. In the future, after ground truth-based training, an ML algorithm may be able to automatically extract radiomic features that identify lung cancer and metastases in micro-CT images. We identified certain numerical parameters that may serve to train ML models. As the precise geometry, position, and orientation of each feature are known in advance, such an approach may be significantly better than manual data labeling in terms of accuracy and robustness. Ultimately, micro-CT may be capable of automatically detecting NSCLC metastases.

Conclusions

Micro-CT was found to be very useful and non-destructive for analyzing whole FFPE block, including LN metastases. Our findings indicate that the quantitative structural variables obtained through micro-CT effectively differentiate between tumoral and non-tumoral areas within FFPE block from mediastinal LNs. This pilot study, offering a new and numerical point of view, may pave the way for the development of an artificial intelligence algorithm. Nevertheless, further investigations with larger sample sizes are imperative to solidify these findings.

Financial Disclosure

The authors have no funding to disclose

Author Contribution

Study Design: AKC, KO, SDS
Data Collection: AKC, SGG, HÖ, YK
Statistical Analysis: KO, DK
Data Interpretation: AKC, KO, SDS, DK
Manuscript Preparation: AKC, KO, SDS, DK, SGG, HÖ, YK
Literature Search: AKC, SGG, HÖ,YK

Data statement / Availability of data and material

Information on the data is provided by the authors if necessary.

Declaration of competing interest

The authors declare no conflict of interest.

Appendix A. Supplementary data

Supplementary data to this article can be found online at https://doi.org/10.1016/j.jpi.2024.100373.

References

1. Siegel RL, Miller KD, Fuchs HE, Jemal A. Cancer statistics, 2022. CA Cancer J Clin 2022;72:7-33.
2. NCCN Clinical Practice Guidelines in Oncology. *Non-Small Cell Lung Cancer Version 2.2024*. February 9, 2024.
3. Huang J, Osarogiagbon RU, Giroux DJ, et al. The InternArticles in press. ational Association for the Study of Lung Cancer Staging Project for Lung Cancer: proposals for the revision of the N descriptors in the forthcoming ninth edition of the TNM classification for lung cancer. J Thoracic Oncol 2024. Articles in press. https://doi.org/10.1016/j.jtho.2023.10.012.
4. Bradbury P, Sivajohanathan D, Chan A, et al. Postoperative adjuvant systemic therapy in completely resected non-small-cell lung cancer: a systematic review. Clin Lung Cancer 2017;18:259–273.
5. Arriagada R, Bergman B, Dunant A, et al. Cisplatin-based adjuvant chemotherapy in patients with completely resected non-small-cell lung cancer. N Engl J Med 2004;350:351–360.
6. Ou SH, Zell JA, Ziogas A, Anton-Culver H. Prognostic factors for survival of stage I nonsmall cell lung cancer patients: a population-based analysis of 19,702 stage I patients in the California Cancer Registry from 1989 to 2003. Cancer 2007;110:1532–1541.
7. Raz DJ, Zell JA, Ou SH, et al. Natural history of stage I non-small cell lung cancer: implications for early detection. Chest 2007;132:193–199.
8. Rena O, Oliaro A, Cavallo A, et al. Stage I non-small cell lung carcinoma: really an early stage? Eur J Cardiothoracic Surg 2002;21:514–519.
9. Goldstraw P, Chansky K, Crowley J, et al. The IASLC lung cancer staging project: proposals for revision of the TNM stage groupings in the forthcoming [eighth] edition of the TNM classification for lung cancer. J Thorac Oncol 2016;11(1):39–51.
10. Osarogiagbon RU, Allen JW, Farooq A, Wu JT. Objective review of mediastinal lymph node examination in a lung cancer resection cohort. J Thorac Oncol 2012;7(2):390–396.
11. Dai CH, Li j, Yu LC, Li XQ, Shi SB, Wu JR. Molecular diagnosis and prognostic significance of lymph node micrometastasis in patients with histologically node-negative non-small cell lung cancer. Tumor Biol 2013;34:1245–1253.
12. Xu B, Teplov A, Ibrahim K, et al. Detection and assessment of capsular invasion, vascular invasion and lymph node metastasis volume in thyroid carcinoma using micro CT scanning of paraffin tissue blocks [3D whole block imaging]: a proof of concept. Mod Pathol 2020 Jul 2. https://doi.org/10.1038/s41379-020-0605-1.
13. Wang S, Yang DM, Rong R, Zhan X, Xiao G. Pathology image analysis using segmentation deep learning algorithms. Am J Pathol 2019;189(9):1686–1698.

14. Orhan K, Jacobs R, Celikten B, et al. Evaluation of threshold values for root canal filling voids in micro-CT and nano-CT images. Scanning 2018:9437569. https://doi.org/10.1155/2018/9437569.
15. Guldberg RE, Ballock RT, Boyan BD, et al. Analyzing bone, blood vessels, and biomaterials with microcomputed tomography. IEEE Eng Med Biol Mag 2003;22(5):77–83.
16. Orhan K. *Micro-computed Tomography [micro-CT] in Medicine and Engineering.* Springer Nature Switzerland AG. 2020. https://doi.org/10.1007/978-3-030-16641-0. ISBN: 978-3-030-16640-3.
17. Shearer T, Bradley RS, Hidalgo-Bastida LA, Sherratt MJ, Cartmell SH. Three-dimensional visualization of soft biological structures by X-ray computed microtomography. J Cell Sci 2016;129(13):2483–2492.
18. Kampschulte M, Schneider CR, Litzlbauer HD, et al. Quantitative 3D micro-CT imaging of human lung tissue. Fortschr Röntgenstr 2013;185:869–876.
19. Descamps E, Sochacka A, de Kegel B, Van Loo D, Hoorebeke L, Adriaens D. Soft tissue discrimination with contrast agents using micro-ct scanning. Belgian J Zool 2014;144(1):20–40.
20. Ritman EL. Micro-computed tomography of the lungs and pulmonary-vascular system. Proc Am Thorac Soc 2005;2:477–480.
21. Bompoti A, Papazoglou AS, Moysidis DV, et al. Volumetric imaging of lung tissue at micrometer resolution: clinical applications of micro-CT for the diagnosis of pulmonary diseases. Diagnostics 2021;11:2075.
22. Cecchini MJ, Tarmey T, Ferreira A, et al. Pathology, radiology, and genetics of interstitial lung disease in patients with shortened telomeres. Am J Surg Pathol 2021;47:871–884.
23. Cavanaugh D, Johnson E, Price RE, Kurie J, Travis EL, Cody DD. In vivo respiratory-gated micro-CT imaging in small-animal oncology models. Mol Imaging 2004;3(1):55–62.
24. Senter-Zapata M, Patel K, Bautista PA, Griffin M, Michaelson J, Yagi Y. The role of micro-CT in 3D histology imaging. Pathobiology 2016;83:140–147.
25. Farahani N, Braun A, Jutt D, et al. Three-dimensional imaging and scanning: current and future applications for pathology. J Pathol Inform 2017;8:36.2017 Sep 7: https://doi.org/10.4103/jpi.jpi_32_17.
26. Buffiere JY, Maire E, Adrien J, Masse JP, Boller E. In situ experiments with X-ray tomography: an attractive tool for experimental mechanics. Exp Mech 2010;50:289–305.
27. Amrhein S, Rauer M, Kaloudis M. Characterization of computer tomography scanners using the probability of detection method. J Nondestruct Eval 2014;33:643–650.
28. Wang L, Yuan K, Luan X, Li Z, Feng G, Wu J. 3D characterizations of pores and damages in C/SiC composites by using X-ray computed tomography. Appl Compos Mater 2018;26:493–505.
29. Kayı Cangır A, Dizbay Sak S, Güneş G, Orhan K. Differentiation of benign and malignant regions in paraffin-embedded tissue blocks of pulmonary adenocarcinoma using micro-CT scanning of paraffin tissue blocks: a pilot study for method validation. Surg Today 2021;51(10):1594–1601.
30. Dizbay Sak S, Sevim S, Buyuksungur A, Kayı Cangır A, Orhan K. The value of micro-CT in the diagnosis of lung carcinoma: a radio-histopathological perspective. Diagnostics 2023;13:3262.
31. Feldkamp LA, Goldstein SA, Parfitt AM, Jesion G, Kleerekoper M. The direct examination of three-dimensional bone architecture in vitro by computed tomography. J Bone Miner Res 1989;4(1):3-11. https://doi.org/10.1002/jbmr.5650040103.
32. Mishaela R, Rubin MD, John P, Bilezikian MD. Anabolic therapy of osteoporosis in women and men. In: *Legato MJ, ed. Principles of Gender-Specific Medicine. California: Elsevier Academic Press; 2004. p. 995-1009.[Chapter 92].*
33. De Oliveira KMH, Nelson-Filho P, Da Silva LAB, Küchler EC, Gatón-Hernandez P, Da Silva RAB. Three-dimensional micro-computed tomography analyses of induced periapical lesions in transgenic mice. Ultrastruct Pathol 2015;39:402–407.
34. Yeom HR, Blanchard S, Kim S, Zunt S, Chu TMG. Correlation between micro-computed tomography and histomorphometry for assessment of new bone formation in a calvarial experimental model. J Craniofac Surg 2008;19(2):446–452.
35. Rüegsegger P, Koller B, Müller R. A microtomographic system for the nondestructive evaluation of bone architecture. Calcif Tissue Int 1996;58(1):24–29.
36. Müller R, Van Campenhout H, Van Damme B, et al. Morphometric analysis of human bone biopsies: a quantitative structural comparison of histological sections and micro-computed tomography. Bone 1998;23(1):59–66.
37. Chappard D, et al. Comparison insight bone measurements by histomorphometry and micro-CT. J Bone Miner Res 2005;20(7):1177–1184.